Preparation and Ablation Performance of Lightweight Phenolic Composite Material under Oxyacetylene Torch Environment

Issam Elwan[1], Rafi Jabra[1], Mohamed Hamzeh Arafeh[1]

Elwan I http://orcid.org/0000-0002-9647-9372

Jabra R http://orcid.org/0000-0003-0227-9263

Arafeh MH http://orcid.org/0000-0002-8696-8586

ABSTRACT: The present study investigates the influence of fiber content on thermal properties of short silica fiber (SSF) reinforced modified resole resin (MRR) composites. For this purpose, different SSF loading composites were prepared: 40, 55, and 65 wt.%. The ablation resistance related to mass loss parameters was quantified by testing under an oxyacetylene flame up to 2300 °C for 30 s. The thermal conductivity of the composite was studied via experimental steady state technique. Thermal stability of the composite material was estimated by means of thermo-gravimetric analysis (TGA), both in air and nitrogen atmosphere. The ablated composite material was characterized by different techniques (XRD, FTIR, and SEM). The results showed that the back-face surface temperature of SSF/MRR composites follows the typical variation curve, and linear ablation rate, mass ablation rate, and char yield decrease with increasing silica fiber content. This confirms that 55 and 65 wt.% SSF loading exhibited the best anti-ablation performance and the lowest percentage of char yield. XRD and FTIR analysis of the ablated specimen zone showed the absence of new phase. The thermo-gravimetric analysis confirmed the thermal resistance of SSF/MRR composites in comparison with MRR matrix and the decrease of char with increasing SSF loading. The thermal conductivity of these composites was significantly enhanced by the SSF into the modified resole matrix. This thermal conductivity follows both the rule of mixture and Maxwell models. The overall thermal characteristics of the SSF/MRR composites meet most of the necessary high temperature application criteria.

KEYWORDS: Ablation properties, Modified resole resin, Short silica fiber, Thermal conductivity.

INTRODUCTION

Fiber-reinforced composites have received much attention as ablative materials for aerospace applications in recent years (Eslami *et al.* 2015). The choice of reinforcing fiber and matrix depends upon various factors, among which strength, thermal stability, load bearing capability, and most importantly the type of envisaged application. Ablative composites are those materials that sacrifice themselves to protect the inner hardware during vehicles and spacecraft's reentry from ultrahigh temperature and supersonic environments (Hu *et al.* 2014). The ablation of a material depends on its inherent properties and also on extrinsic conditions such as thermal, chemical, and mechanical factors related to theoretical or practical environment variables. When studying thermal behavior of phenolic-silica composites, it has to be noted that the most important subject is the decomposition

behavior of the matrix, since reinforcing silica fibers have very much higher thermal stability than the polymeric matrix. Therefore, phenolic resins are considered among the best matrix for advanced composites providing the unbeatable combination of handling characteristics, processing flexibility, composite mechanical properties and acceptable cost. Resole type phenolic resin has attracted great scientific interest as it can be effectively used as a matrix system in ablation resistant composites due to its excellent erosion resistance and char retention capacities (Bahramanian *et al.* 2006). Its properties can be further improved by modification with different additives like polyvinyl butyral (PVB), which improves processability and toughness (Kang and Hwang 1996). Resole resin falls under the category of thermosetting ablators, which are also known as non-melting, char forming resins and possessing high heat of pyrolysis. Thus, during fire exposure, phenolic resin receives heat in the initial stage, decomposes to char and forms a thermal insulation layer. The large number of aromatic rings in the resole type phenolic resin leads to high carbon yield and the effective char formation ability (Mouritz and Gibson 2006). High char retention of the resole type phenolic resins makes them an effective candidate for ablative nozzle liner application (Nair 2004; Hu *et al.* 2014). To further increase the thermal stability of the composite, chopped silica fiber (SSF) was considered as reinforcing filler because of its high thermal resistance and melting temperature above 1700 °C. SSF has also a very low coefficient of thermal expansion (0.54×10^{-6} K^{-1}) and low thermal conductivity (0.65 W/m.K), which make it suitable for applications including ablators and thermal barriers (Wang *et al.* 2012; Shulock and Saffadi 1982).

Phenolic-silica composites are considered as one of the most important classes of ablative material of high temperature for high specific heat, low density, small ablation rate, and high rate of carbon conversion utilized more extensively in structure and ablation applications (Shi *et al.* 2015). When such an ablative material is subjected to high-heat flux, the phenolic resin within the composite will pyrolyze at first. As the pyrolysis proceeds, the decomposition zone will recess and penetrate the material (Shi *et al.* 2016a). The products of the pyrolysis are a mixture of gasses and residual char layer of carbon and silica mainly. If the heat flux is very large, the silica fiber will eventually melt forming liquid film covering some char surface. The pyrolysis gasses will then percolate through the char and bubble through the molten layer. In this process, complex post-pyrolytic chemical reactions may also take place. Near the surface of the molten layer, heterogeneous carbon-silica reactions may occur and molten silica may be subject to vaporization (Shi *et al.* 2016b; Hsieh and Seader 1973). In addition, the char plays an important role in ablation process by limiting oxygen diffusion from the boundary layer to the bulk and retarding exothermic degradation reactions of the polymeric matrix (Hsieh and Seader 1973). Torre *et al.*, in their studies on a silica-based ablative composite, found that the char produced from the degradation of polymeric ablators was weak, brittle, and therefore, susceptible for rapid removal by the mechanical stresses due to the high vehicle speed, this phenomenon provokes the reduction of the thermal insulation (Torre *et al.* 2000; 1998a). Therefore, reinforcing fibers and other inorganic fillers must be included in the ablative formulation in order to improve the char stability and imparts mechanical strength to the char formed after the degradation of the polymer matrix. Shi *et al.* (2015) investigated thermal decomposition behavior of silica-phenolic composite by using solar radiant heating experiment with one-sided heat flux. They found that silica-phenolic composite exhibited an excellent thermal insulation during thermal exposure.

The aim of the present study was primarily to understand thermal and ablative properties under oxy-acetylene torch exposure environment of short silica fibers (SSF) modified resole resin (MRR) composites with different percentage of random SSF prepared by hot pressing technique. The effect of SSF concentration on the thermal decomposition/ablation and back-face temperature elevation of SSF/MRR composites are herein investigated. Ablation characteristics of SSF/MRR composites were studied by scanning electron microscopy (SEM), X-Ray diffraction (XRD), and FTIR spectroscopy.

MATERIALS AND METHODS

Phenol (HS Code 2907 11 00) and formaldehyde (HS Code 2912 11 00) monomers, concentrated sulfuric acid (HS Code 2807 00 00), absolute ethanol (HS Code 2207 10 00) and ammonia solution 25% (HS Code 2814 20 00) were obtained from Merck. Zinc stearate (Technical grade) was supplied by Sigma-Aldrich. Polyvinyl butyral was purchased from Wacker Co., Germany, under the trade name Pioloform BM18 with butyral and hydroxyl content of 80 wt.% and 18 ± 1.5 wt.%, respectively, and employed for

improving the toughness of resole resin. Silicon spray lubricant (WD40) was used to facilitate specimen de-molding. Chopped silica fibers manufactured by JSC Polotsk-Steklovolokno, Republic of Belarus, under the trade name PS-23 (9) were used as reinforcement material and their properties are shown in Table 1. The ammonia type resole phenolic resin was synthesized in the authors' laboratory.

Table 1. Physical properties of chopped silica fiber.

Property	Value
Product Code	PS-23 (9)
Fiber length	4 – 24 ± 1 mm
Density	2.2 g/cm³
Heat capacity	1220 J/kg.K
Thermal conductivity	0.65 W/m.K
Nominal diameter of elementary filament	9 ± 1 μm
Moisture contents	not more than 3,5 %
SiO_2 content	96 % min
Loss on ignition	7 – 12 %
Temperature Resistance	> 1000 °C

PREPARATION OF AMMONIA TYPE RESOLE PHENOLIC RESIN

Resoles are phenol-formaldehyde condensation products with methylol groups and final cured structure with a random three-dimensional network of aromatic rings. Resole type thermoset was synthesized via polymerization of phenol and formaldehyde using NH_4OH as a catalyst (Shafizadeh *et al.* 1999). Formaldehyde (F) and phenol (P) were mixed in the molar ratio of F/P = 1.25 with 0.15 mole catalyst. Four necks round bottom flask equipped with mechanical stirrer, temperature controller, and condenser was charged with 1 mole of phenol, 1.25 mole of 37% aqueous formaldehyde solution and 5.25 g of ammonia solution which was added dropwise giving a complex 3-D network. The solution was stirred and refluxed for 75 min at 85 °C. Then pH value was adjusted to 6 – 7 by the addition of 5% sulfuric acid solution. The aqueous phase was decanted, and the rest of water was removed by distillation under reduced pressure for about 3 h at 60 °C. Figure 1 shows the condensation reaction of ammonia resole resin. The physical properties of prepared ammonia resole resin are tabulated in Table 2.
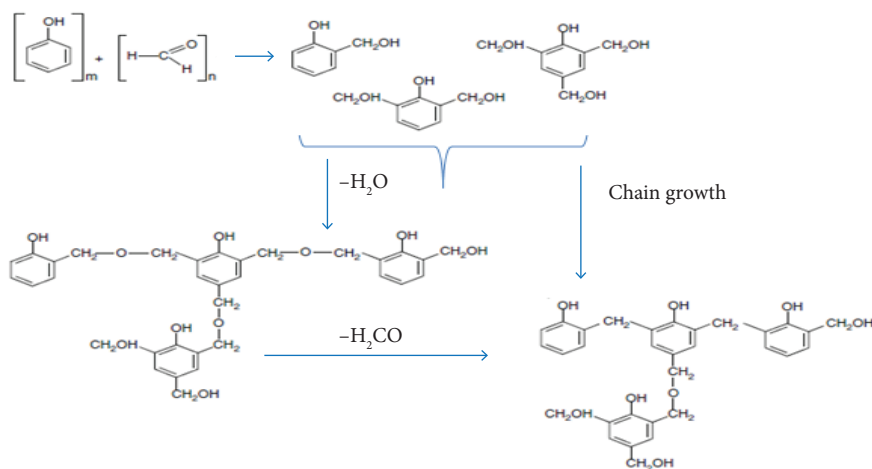

Figure 1. Schematic reaction mechanisms for resole resin condensation (Pilato 2010).

As demonstrated in Fig. 1, the condensation reaction result is mostly resole resin, water and formaldehyde.

Table 2. Physical properties of synthesized resole resin type ammonia.

Property	Value
Physical form	Clear brown liquid
Solid content	77 – 79 %
Gel time at 150 °C	100 – 110 s
Density	1.12 g/cm^3
pH	7.1 – 7.4
Content of free phenol	6.41 %
Content of free formaldehyde	3.25 %
Heat capacity	2000 J/kg.K
Thermal conductivity	0.19 – 0.21 W/m.K

IMPREGNATION SOLUTION PREPARATION

First of all, the solid content of prepared phenolic resole resin was adjusted to be 50 wt.% using absolute ethanol. Then, it was blended with PVB at a level of 15 parts per hundred weights of resin (phr) using absolute ethanol as common solvent. Blending was done using laboratory mixer (G-250 Laboratory Mixer) at 30 °C and stirrer speed of 200 rpm for 2 h. Then, 2 wt.% zinc stearate as release agent was added to the solution under mixing for additional 20 min at room temperature. The viscosity of the impregnation solution was measured using Ford cup Ø4 and adjusted using absolute ethanol to be 40 – 50 s.

PREPARATION OF COMPOSITE SPECIMENS

The fabrication of SSF/MRR composite specimens consists of a series of operations including mixing, hydraulic pressing, curing, post curing and finishing. Three types of samples were made for material testing. The compositions, expressed as SSF/MRR wt./wt. of 40/60, 55/45, and 65/35 were blended in a laboratory mixer (G 250). Prior to mixing chopped silica fibers were dried in the oven at 100 °C for about 3 h to remove all its humidity. Initially, the chopped silica fibers are immersed in impregnation solution and mixed together for 60 min using a mechanical stirrer at 150 rpm until silica fibers are fully impregnated. Due to the importance of the mixing process and its great influence on the final properties of short silica fiber composites, the samples were mixed for sufficient time to disperse the fibers in the matrix solution and prevent fiber's agglomeration. Subsequently, the prepared composite mixture was spread on a stainless plate and allowed to dry in air at room temperature for 24 h, then, put into the oven at 60 °C for 6 h to remove the solvent. The resultant composite mixture was molded into various specimens for testing and characterization using the hot compression molding technique with a press of 50 ton capacity. Initially, the mold was coated with a thin layer of silicone spray lubricant (WD40) and filled with dried composite mixture, then, the die was assembled and closed. The constant cure cycles for all specimens were done by heating under pressure in the mold. The molding, heating and pressing cycle were performed according to the following cure profile: heating from room temperature to 130 °C with heating rate 4 °C/min at ordinary pressure, then, 10 MPa pressure application at 130 °C and dwell time of 30 min. In the next step, the temperature was increased to 160 °C with heating rate 1 °C/min under the same pressure for 30 min at this temperature. Finally, the molded composite was cooled under the same pressure to ambient temperature with cooling rate 3 °C/min. Figure 2 shows molding and cure cycle. Subsequently, the applied pressure is released, the sample is removed from the die, the produced composite trimmed and then post cured at 170 °C for 120 min. The post curing operation was done to complete resin cure and achieve better chemical, mechanical and thermal properties (Da-Peng and Hong 2008).
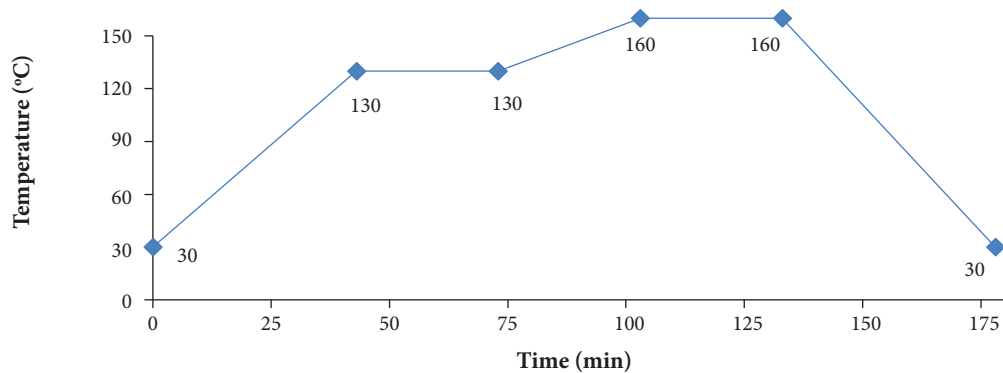
Figure 2. Molding and cure cycle procedure for SSF/MRR composites.

CHARACTERIZATION

ABLATION TESTING, BACK-FACE TEMPERATURE EVALUATION AND INSULATION INDEX

To study the ablation behavior of the composites, the severe hyperthermia environment was simulated by the oxyacetylene torch test according to ASTM E285-80 standard. A mixture of oxygen and acetylene was fired and used as the heat source of the experimental platform for ablation. Plate test specimens were of 100×100 mm in size and 7 mm in thickness. The nozzle diameter of the torch was 2 mm. The distance and the angle between the specimen surface and the torch tip were 20 mm and 90°, respectively. One K-type thermocouple was firmly attached at the center of the back-face of the specimen to record continuously temperature changes as a function of time during ablation test. This temperature sensing device was connected to the data logger laptop. The flow rates of oxygen and acetylene were 1.36 m^3/h and 1.04 m^3/h, respectively, which generated a flame temperature of around 2400 °C during the test. This device is able to produce a high-temperature flame of approximately 3000 °C and high heat flux of about 820 W/cm^2. A schematic of the torch test facility is shown in Fig. 3.
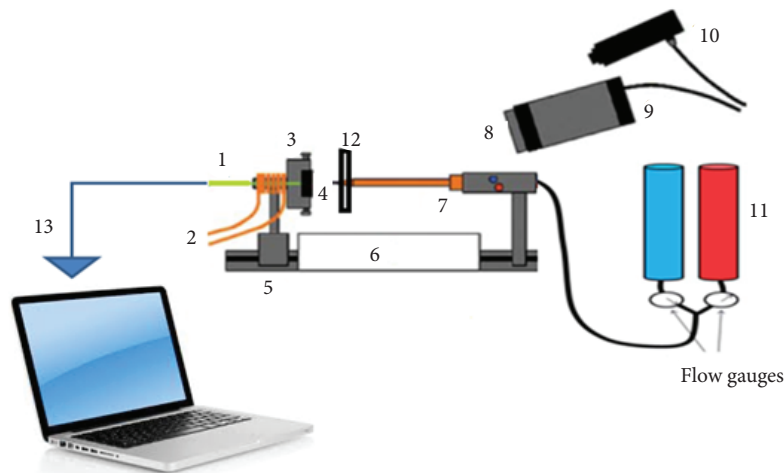

Figure 3. Oxyacetylene torch apparatus used for composite ablation: (1) back face thermocouple; (2) water cooling system; (3) specimen holder; (4) specimen; (5) specimen guide; (6) protective insulation; (7) oxyacetylene torch; (8) neutral filter; (9) thermal imaging camera; (10) pyrometer; (11) gas cylinders; (12) thermal barrier; and (13) data logger laptop.

Prior to the ablation test, the samples were machined and grounded so as to obtain high parallel surfaces between the top and the bottom. Sample thickness was monitored using digital gauge disc caliper micrometer. The ablation test was continuously performed until the specimen was burnt through its entire thickness during a defined time to calculate insulation index and

erosion rate. In order to measure the linear and mass ablation rates, samples were held for 30 s and then the flame was extinguished allowing the samples to cool down naturally. The thickness and mass changes of all samples during the test were divided into the exposure time. The linear (LAR) mass (MAR) ablation rates, insulation index (I_T), and percentage char yield were calculated according to the Eqs. 1-4.

$$\text{Linear ablation rate (LAR) (mm/s)} = \frac{T_0 - T_1}{t} \tag{1}$$

$$\text{Mass ablation rate (MAR) (g/s)} = \frac{M_0 - M_1}{t} \tag{2}$$

$$\text{Insulation index (s/m)} = I_T = \frac{t_T}{T_0} \tag{3}$$

$$\% \text{ Char yield} = \left[\frac{M_0 - M_1}{M_0} \right] \times 100 \tag{4}$$

where: T_0, M_0, T_1 and M_1 are the thickness and mass of the ablator specimen before and after ablation testing, respectively; t is the ablation time fixed at 30 s; and t_T is the burn-through time (s) representing the time required to completely pierce the specimen. The schematic illustration for calculating linear ablation rate is presented in Fig. 4. Thickness measurements of ablated samples (T_1) were done using the same digital gauge disc caliper micrometer.

Figure 4. Scheme for calculating linear ablation rate.

Figure 5 shows the images of one of the composite samples taken during the oxyacetylene torch testing and immediately after extinguishing the flame. Flame zones, namely primary flame zone and reflected flame zone, cover the entire surface area of the specimen. It is a very aggressive test because it involves high-temperature, high-velocity gas flow, and oxidizing gases.
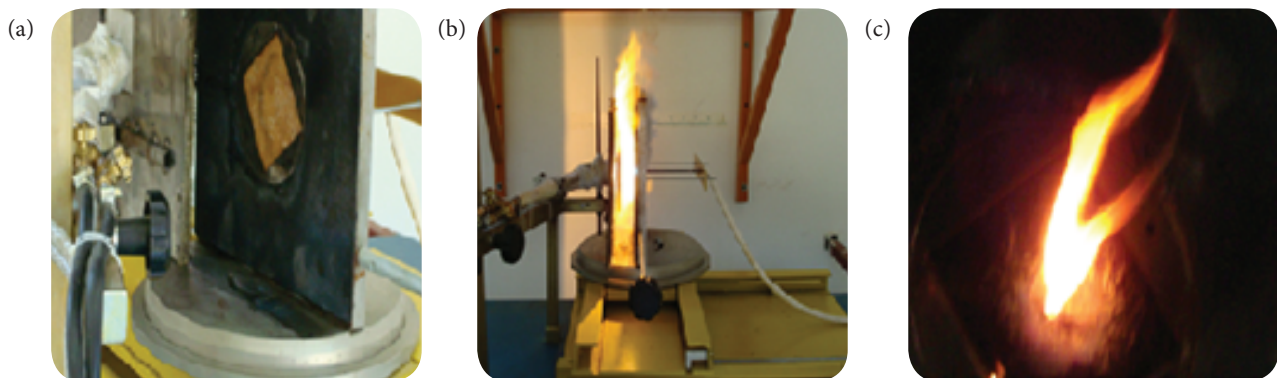

Figure 5. Oxyacetylene test: (a) sample placed over a steel platform; (b) testing under an oxyacetylene flame at 20 mm from the nozzle; and (c) sample just after ablation.

ABLATED COMPOSITE X-RAY DIFFRACTION ANALYSIS

Carbonized SSF/MRR composites were analyzed by X-Ray diffraction (XRD). The XRD characterization was performed using a classical diffractometer Philip PW 3710, type Bragg-Brentano θ-2θ, with negligible instrumental broadening using Cu Kα radiation (λ = 0.15406 nm) in the range 2θ = 10° – 80°, using a step size of 0.02, 40 kV and 30 mA.

ABLATED COMPOSITE FTIR SPECTROSCOPY ANALYSIS

Different functional groups and structural features of carbonized SSF/MRR composites were identified using FTIR spectroscopy. Studies were carried out using a Bruker Vector 22 FTIR Spectrometer with a standard DTGS and KBr window. Spectra were recorded in a range of 4500 – 400 cm^{-1}, with a resolution better than 1 cm^{-1}. The spectra of testing samples were produced at room temperature using a transmission technique with KBr pellet.

COMPOSITE AND MODIFIED RESOLE RESIN THERMO-GRAVIMETRIC ANALYSIS

The thermal decomposition is defined by the American Society for Testing and Materials (ASTM) as "a process of extensive chemical species change caused by heat", it involves physical as well as chemical processes. The physical processes entail charring, decomposition change and burning characteristics of the material, whilst chemical processes are responsible for the generation of flammable volatiles (Wilkie and Morgan 2009). Thermal stability of SSF/MRR composites and matrix carbonization with respect to temperature were evaluated using a thermo-gravimetric analyzer (TGA) (SETARAM LABSYS evo TGA 1150 Instruments, France) as per ASTM E1868. Samples of 10 – 20 mg were heated from 30 °C to 1100 °C at a heating rate of 10 °C/min. The TGA tests were performed in normal atmosphere environments and in nitrogen (N_2) separately. According to the initial sample weight and degradation temperature, sample percentage char was recorded.

COMPOSITES THERMAL CONDUCTIVITY TEST

Thermal conductivity (λ) is defined as the ability of the material to transmit heat, it is measured in watts per square meter of surface area for a temperature gradient of 1 K per unit thickness of 1 m. The thermal conductivity is not always constant. The main factors affecting thermal conductivity are the material density and moisture and the test temperature. With increasing density, moisture and temperature, the thermal conductivity also increases (Chen *et al.* 2016). Measurement of thermal conductivity was performed by utilizing the thermal conductivity meter DTC-25 (TA Instruments, USA) for quick determination of thermal conductivity of solid materials using the guarded heat flow method. The TA Instruments DTC-25 thermal conductivity meters measures thermal conductivity according to the ASTM E1530 guarded heat flow meter method. In this technique, a sample of the material with 50 mm in diameter and 5 mm in thickness is held under a compressive load between two surfaces, each controlled at a different temperature. The lower surface is part of a calibrated heat flux transducer. As heat is transferred from the upper surface through the sample to the lower surface, an axial temperature gradient is established in the stack. By measuring the temperature difference across the sample along with the output from the heat flux transducer, thermal conductivity of the sample can be determined when the thickness is known. Knowing the values of supplying heat, temperatures and thickness, the thermal conductivity is determined by employing one-dimensional Fourier's conduction law (Eq. 5). All measurements were performed at 30 ± 1 °C.

$$Q = -\lambda A \frac{dT}{dx}$$

(5)

where: *Q* is the heat flow conduction rate (W); λ is the thermal conductivity of the specimen (W/m.K); *A* is the cross-sectional area normal to heat flow direction (m^2); and *dT*/*dx* is the temperature gradient (K/m) determined from the plotted graph of temperature versus time.

MODELING OF COMPOSITE THERMAL CONDUCTIVITY

Thermal conductivity is a bulk property. Estimation of thermal conductivity of short fiber composites has been the subject of numerous analytical and empirical models, but none of them appears to characterize all types of composites (Fu and Mai 2003). In this paper, the review of thermal conductivity analytical models of composite materials is out of scope, but the focus was directed to one analytical model that is widely used in literature for comparison with experimental data. For a two component composite material, the simplest alternative would be to consider the material arranged either in parallel or in series with respect to the heat flow direction (Fig. 6), this leads to the upper and lower bounds of the effective thermal conductivity. In this study, we found that our experimental results could fit remarkably with models such as the rule of mixture one (Eq. 6) and the Maxwell's model (Eq. 7) (Chikhi *et al.* 2011), which describe very well the conductivity of randomly distributed and non-interacting homogeneous spheres in a homogeneous medium.

$$\lambda^n = V_f \lambda_f^n + (1 - V_f) \lambda_m^n \tag{6}$$

$$\lambda = \lambda_m \left[\frac{2\lambda_m + \lambda_f - 2(\lambda_m - \lambda_f)V_f}{2\lambda_m + \lambda_f + 2(\lambda_m - \lambda_f)V_f} \right] \tag{7}$$

where: n = 1 for parallel conduction model; n = –1 for series conduction model; V_f is the volume fraction of fiber; λ_f and λ_m are thermal conductivity of fiber and matrix, respectively.

We will see that our experimental points could adapt very well with such models better than other models like Russell's (Shen *et al.* 2011). However, the series model seems to be in excellent agreement with experimental data as compared to the parallel model (Bigg 1986). This is because the fibers are gathered in the polymer to form a conductive block of polymer whose alignment is parallel to the direction of thermal flux (parallel conduction). On the other hand, if the alignment of the conductive block of the polymer is perpendicular to the direction of thermal flux, the thermal conductivity will be the lowest (series conduction).
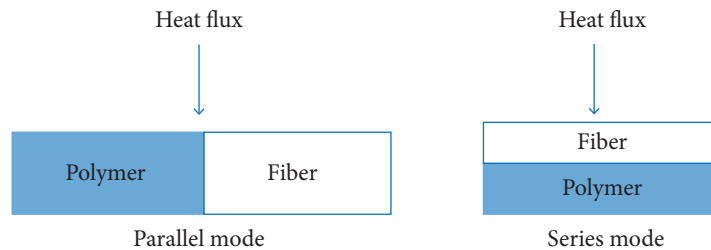

Figure 6. Representation of heat flow in composite materials.

ABLATED COMPOSITES SCANNING ELECTRON MICROSCOPY (SEM) EXAMINATION

The morphology behavior of the ablated composites was observed using VEGA II XMU SEM (TESCAN Company, USA) scanning electron microscopy (SEM). Specimens were sputter-coated with a gold layer before the examination, and the morphology micrographs of the composites were obtained.

RESULTS AND DISCUSSION

BACK-FACE TEMPERATURE PROGRESSION (BTP) OF ABLATED COMPOSITE AND VISUAL INSPECTION

Figure 7 shows the temperature variation at the back surface of (a) 40 wt.%, (b) 55 wt.%, and (c) 65 wt.% SSF/MRR composites. These temperature variation curves were measured experimentally by the oxyacetylene flame test with heat flux of about 820 W/cm². Temperature recording time was 77 s (30 s exposure time + 47 s post exposure time). At the end of the exposure time, the back surface temperature of a 7 mm thickness 40 wt.%, 55 wt.%, and 65 wt.% composites were 263.09 °C, 67.38 °C, and

42.77 °C, respectively. These results show that the back surface temperature of 40 wt.% composite specimens, for example, is about 6 times and 4 times higher than those of 65 wt.% and 55 wt.% composite specimens, respectively. It can be observed from Fig. 7 that 55 wt.% and 65 wt.% composites behave thermally similarly until 40 s (30 s + 10 s) of flame test. After that, the maximum back-face temperatures of 40 wt.%, 55 wt.% and 65 wt.% composite specimens reach maximum values of 293 °C, 295.9 °C, and 288.3 °C at the 40.5th s, 65.8th s, and 72nd s, respectively. It is observed that BTP was reduced with increasing SSF loading in the SSF/MRR composites. Considering a random distribution for both fiber lengths and fiber orientations (morphology analysis paragraph), it can be concluded that the augmentation of silica fiber fraction to a certain limit in MRR matrix has improved the thermal insulation of SSF/MRR composites with low fiber loading. On pyrolysis, the glassy char layer formed from MRR matrix builds up in the front, forms a protective layer and restricts heat transfer into the material impeding oxygen diffusion into the material. On the other hand, the incorporation of SSF in MRR matrix may act as a heat dissipater or as a much better network for transferring heat in a random manner. Hence, the fiber network will actually act as an additional heat barrier allowing SSF composites to exhibit superior integrity, which is advantageous for the performance of the composite as an ablative thermal protection system (Najim *et al.* 2008).
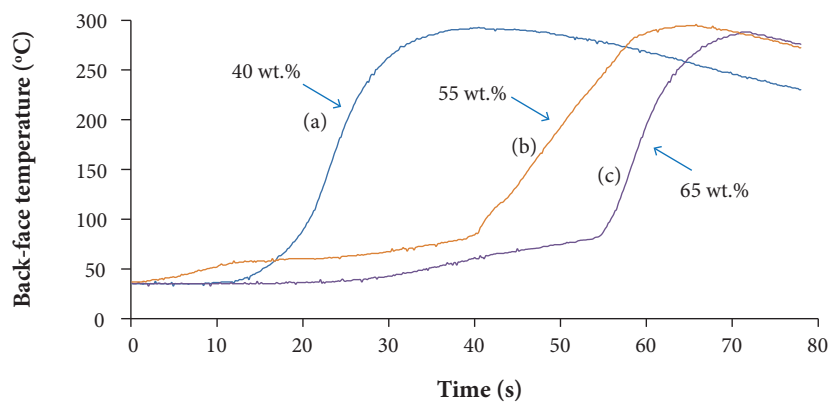

Figure 7. Back-face surface temperature profiles of SSF/MRR composites (a) 40 wt.%, (b) 55 wt.%, and (c) 65wt. % SSF after 30 s exposure to an oxyacetylene flame at 20 mm distance from the nozzle and 820 W/cm² heat flux.

ABLATED COMPOSITE PERFORMANCE AND CHAR YIELD PERCENTAGE

The geometric form and orientation of the SSF were considered to be randomly distributed. The determination of the SSF/MRR composites erosion rate is generally based on a simplifying assumption that all the SSF in the composite are laid in the same direction (Ommati *et al.* 2011). The ablation properties results of SSF/MRR composites are summarized in Table 3. The LAR, MAR, Insulation index and the char yield of the ablated composite specimens were measured using Eqs. 1-4 respectively and plotted in Fig. 8.

Table 3. Ablation properties of SSF/MRR composites as a function of silica fiber weight fraction.

Weight fraction (wt.%)	Thickness before test (mm)	Burn through time (s)	Insulation index (s/mm)	Erosion rate (mm/s)	LAR (mm/s)	MAR (g/s)	Char yield (%)
40	7.19	36	4.94	0.202	0.178	0.834	20.34
55	7.34	48	6.54	0.153	0.106	0.527	10.44
65	7.29	61	8.48	0.118	0.098	0.357	7.69

Figure 8 illustrates that the increase of silica fiber fraction in the composite leads to the gradual decrease of linear and mass ablation rates. LAR decreases from 0.178 to 0.098 mm/s when the silica fiber fraction increases from 40 to 65 wt.%, respectively (Fig. 8). The same observation can be seen for MAR. This result is in line with the findings of Qiu *et al.* (2005) in their investigation

on ablation performance of boron-modified phenolic resin (BPR) with high silica fiber composites. Moreover, the Char yield curve exhibits the same behavior as LAR. The high char yield value for the 40 wt.% SSF composite is mainly due to the higher MRR matrix amount of this material compared with the 65 wt.% SSF. In addition, as can be seen in Table 3, increasing silica fiber contents in composite leads to decreasing its erosion rate from 0.202 to 0.118 mm/s when silica fiber fraction increases from 40 to 65 wt.%, respectively. Conversely, when silica fiber content in the composite increases, the insulation index increases gradually.
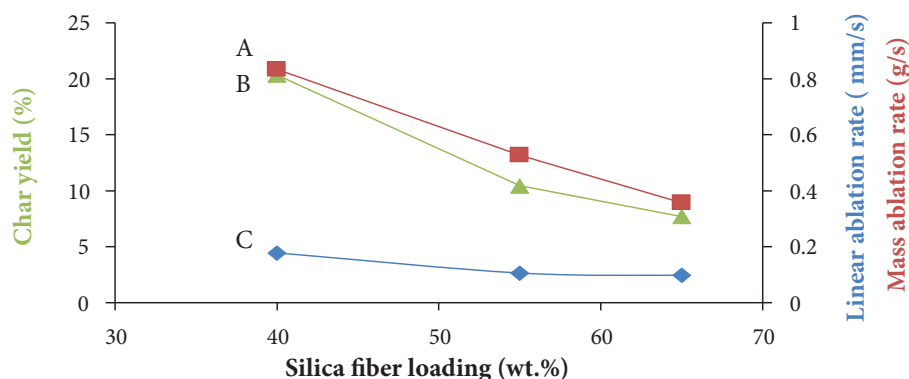

Figure 8. (A) Mass ablation rate; (B) char yield; and (C) linear ablation rate of the ablated composites at different silica fiber loading.

From Table 3 and Fig. 8, it can be concluded that the incorporation of SSF in the MRR matrix enhances the ablation performance. This may be explained on the basis of the thermal diffusivity α (m²/s) = $\lambda/\rho.C_p$, where ρ (Kg/m³) is the density and C_p (J/Kg.K) is the specific heat of the composite; i.e., the smaller α, the better the heat insulation. For low values of material density ρ and thermal conductivity λ, α increases with decreasing C_p value (Qinghua 1992). Compared with other studies (Najim *et al.* 2008), we could say that SSF/MRR composites are exhibiting better insulation than (difurfurylideneacetone (DFA) -resole)/short fiberglass composites.

ABLATED COMPOSITE X-RAY DIFFRACTION PATTERN

The phase structure of ablated SSF/MRR composites has been examined by XRD. Figure 9 gives typical XRD pattern of one ablated composite. A broadband centered at $2\theta = 26.45°$ (3.35 A°) is related to graphite's basal plane (Foley *et al.* 2002) and another lower intensity peak with a maximum at $2\theta = 21.42°$ (4.15 A°) is assigned to amorphous silica (Scian and Volzone 2001). This confirms that, under the performed test conditions, no changes in phase happened after pyrolysis of the SSF/MRR composites since no peaks related to α-cristobalite neither carbon- silica reaction was recognized in the XRD of ablated SSF/MRR composites.
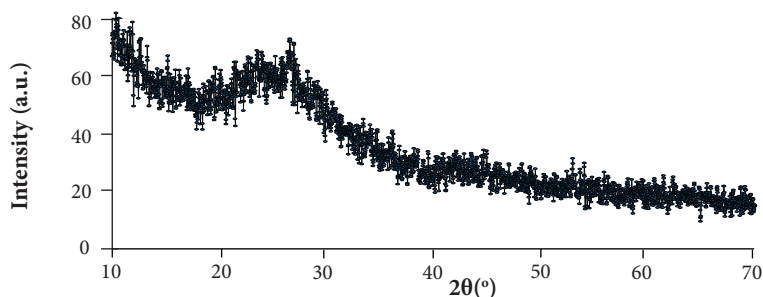

Figure 9. XRD diffractogram of ablated composite.

FTIR ANALYSIS OF ABLATED COMPOSITE

FTIR spectra of carbonized SSF/MRR composite shows four bands as demonstrated in Fig. 10. The band at 465 cm⁻¹ belongs to bending vibration of O-Si-O. The bands from 1090 cm⁻¹ to 1100 cm⁻¹, and from 775 cm⁻¹ to 835 cm⁻¹ belong to O-Si-O stretching

vibrations. The broadband around 3550 cm^{-1} is related to the absorption of Si-OH group, Si-O-Si asymmetrical transversal stretching and surface hydroxyl groups, respectively (Ceballos-Mendivil *et al.* 2014). It is known that all organic materials spectra have small peaks at around 2300 – 2400 cm^{-1} which are related to the effect of C = N, C = O and N = O double bond stretching vibration (Griffiths and Homes 2002).
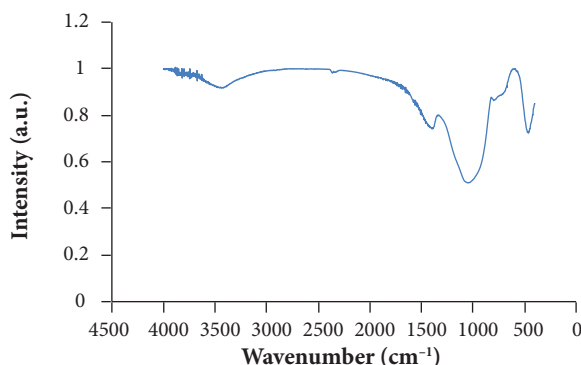

Figure 10. FTIR spectra of ablated SSF/MRR composite.

THERMO-GRAVIMETRIC ANALYSIS

The thermal decomposition behavior of phenolic resins has been studied extensively because of the usage of phenolic matrix composites in high-temperature applications and fire resistant components. One method to reduce the flammability of composites is the addition of inert fillers like silica fiber to the polymer matrix (Lochte *et al.* 1965). TGA curves of MRR matrix, resole resin, and SSF/MRR composite are presented in Figs. 11 and 12, respectively. The general shapes of the three curves are nearly similar. The chemical changes of MRR matrix, resole resin and SSF/MRR composite exhibit a three-stage decomposition behavior that is indicative of a multiple-order decomposition process.

Firstly, a small loss in mass between (100 °C ~ 300 °C) is observed for MRR, resole resin and SSF/MRR composites. This could be attributed to the loss of water resulting from the post curing of phenolic resin during TGA test. At this stage, the polymer network remains highly undamaged and a random three-dimensional network of aromatic rings is obtained through continued condensation of hydroxyl-methyl groups and etherification reaction due to PVB incorporation in the resole resin as illustrated in Fig. 13. This could also lead to increasing the final crosslinking density of resole resin. The total weight loss at this stage is about 2%.

In the second stage and as the temperature increases between (300 °C ~ 650 °C), the MRR matrix, resole resin and SSF/MRR composites undergo thermal degradation and decomposition by scission reactions and formation of phenol, cresols and xylenols resulting from the scission of terminal benzene rings that depend on its position (Trick and Saliba 1995). These reactions are partially oxidative in nature, and the resin itself can act as an oxygen source. The weight loss of MRR matrix, resole resin and SSF/MRR composite at this stage is 39%, 23%, and 16%, respectively. The difference between resole resin and PVB modified resole resin matrix is quite clear in the difference between their weight losses at this second stage. This difference translating the PVB fraction (15 phr) seems not seriously affecting thermal stability of MRR matrix.

The final stage involves further conversion of aromatic rings into a carbonaceous char, with some further evolution of volatiles such as H$_2$, CO, and CH$_4$. In this stage, the aromatic rings of MRR turn into carbonized char by dehydrogenation and hydrogen transfer reaction and the weight loss of MRR matrix, resole resin and SSF/MRR composite is 60%, 60%, and 26%, respectively. These weight losses could be attributed to bulk degradation of modified phenolic resole resin matrix (Kim *et al.* 2016). Above 1000 °C, no significant increase in mass loss is observed because all phenolic resin in the composite has been carbonized and SSF/MRR composite residue reaches 74% approximately at 1150 °C. It is evident that silica fibers induce high effect on SSF/MRR composite char yield and improve thermal stability of MRR matrix (the final weight loss of MRR matrix and SSF/MRR composite are 60% and 26%, respectively).
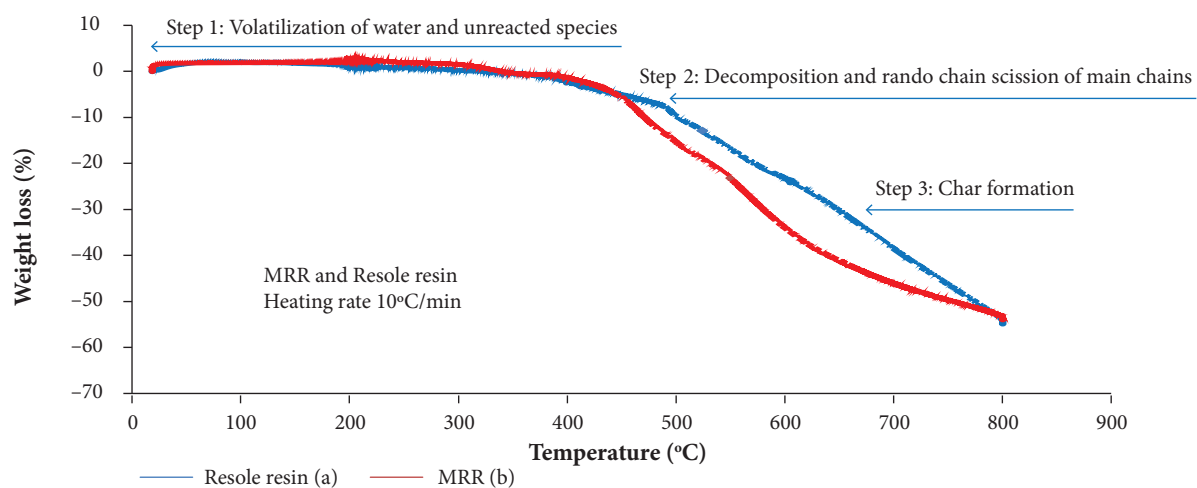
Figure 11. TGA curves of (a) resole resin and (b) MRR matrix in flowing nitrogen (10 °C/min).
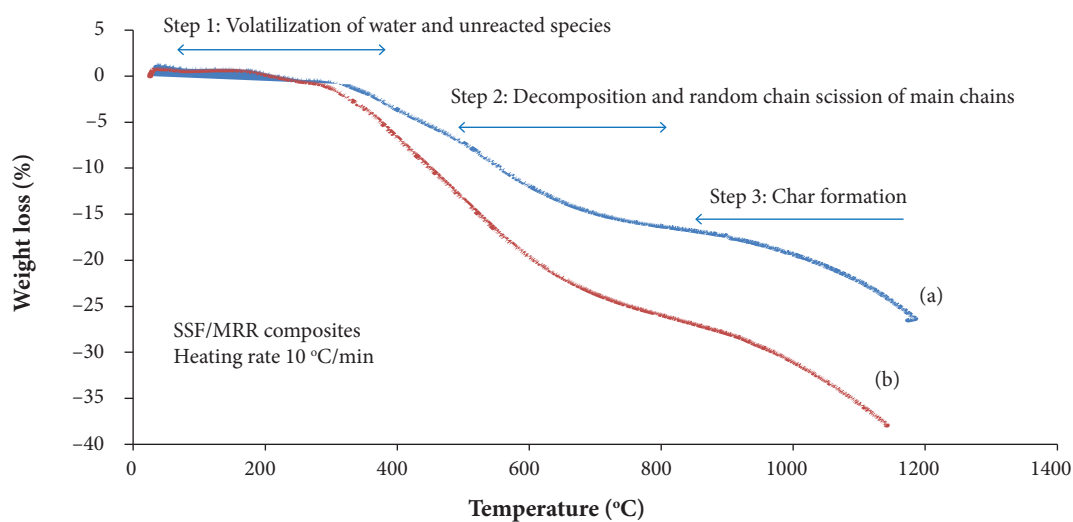

Figure 12. TGA curves for SSF/MRR composites under (a) nitrogen and (b) air flow.
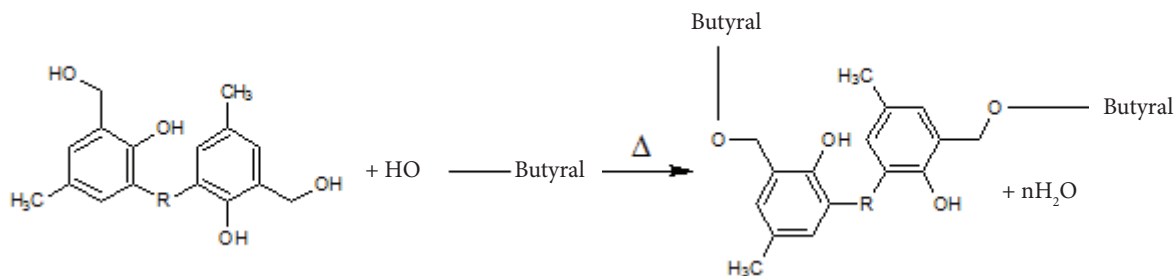

Figure 13. Schematic reaction between PVB and resole resin (Ismail *et al.* 2009).

The simplified illustration of the carbonized structure is represented in Fig. 14. As long as SSF does not decompose at the temperature under test, only modified phenolic resole resin is fully carbonized and transformed into char via dehydrogenation and condensation reactions. Due to the matrix high aromatic content, the yield of flammable volatiles is lower compared to many other polymers, enhancing the superior fire performance and low flammability of phenolic composites (Mouritz and Gibson 2006).
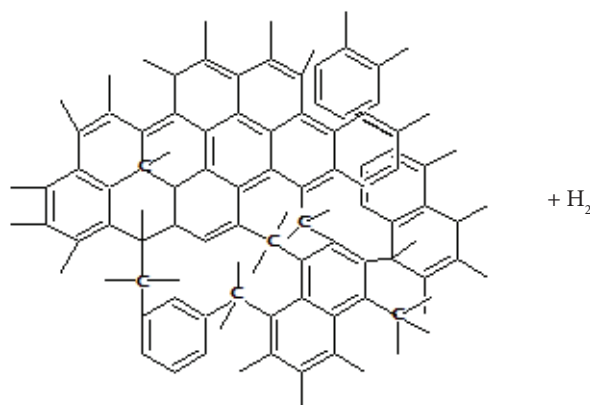

$+ H_2$

Figure 14. Schematic representation of the suggested structure for fully carbonized phenolic resin with highly cross-linked glassy network.

THERMAL CONDUCTIVITY MEASUREMENT

At a specified temperature, the thermal conductivity of fiber reinforced polymer composite materials depends on the properties of the constituents at this temperature as well as their content. As a result, if the temperature-dependent thermal conductivity is known for both fibers and resin, the property of the composite material can be estimated. Thermal conductivities (TC) and densities of SSF/MRR composites at 30 °C are presented in Fig. 15.

The density of SSF/MRR composites increases with increasing fiber loading, the higher density value of 1.64 g/cm³ remains within the reasonable interval of light-weight materials. On the other hand, the thermal conductivity of SSF/MRR composites increases with increasing density and fiber loading. The results show that adding 65 wt.% of silica fiber to MRR increased the thermal conductivity from 0.19 W/m.K to 0.46 W/m.K. It is also seen that composite thermal conductivity and density of composites linearly increase with SSF volume fraction. This is because both thermal conductivity and density of SSF (0.65 W/m.K and 2.2 g/cm³, respectively) are higher than those of MRR (0.19 W/m.K and 1.12 g/cm³, respectively). This could be attributed to the fact that fibers form growing conductive paths in the polymer matrix and increase the thermal conductivity of SSF/MRR composites.
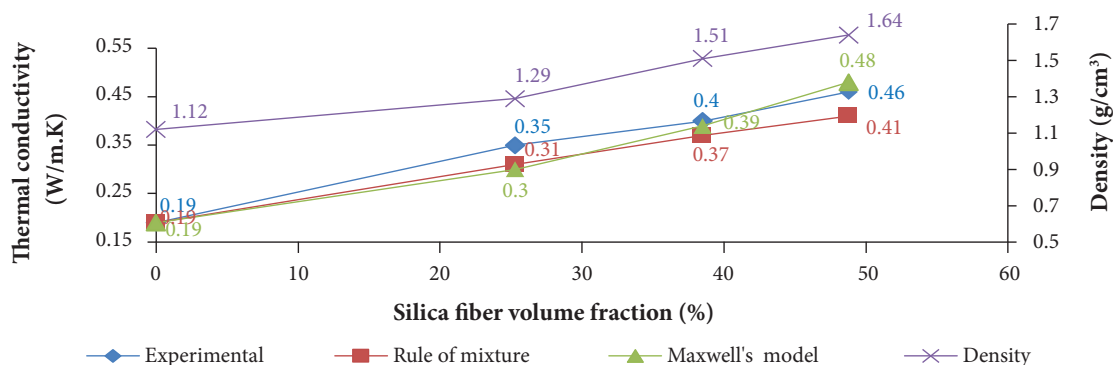

Figure 15. Variation of thermal conductivity and density with SSF volume fraction in SSF/MRR composites.

On the other hand, good distribution of SSF in the composite leads to good thermal dispersion of conducting paths. Figure 15 shows a good agreement between thermal conductivity experimental results and both rule of mixture and Maxwell's models for the prediction of thermal conductivity of similar composite materials. The much lower conductivities of the silica phenolic composites are the result of the ceramic insulating characteristics of these fibers and the dominant heat transfer through phonons rather than free electrons. Generally, most metal oxide fillers such as alumina (Al_2O_3) and silica (SiO_2) have a lower TC (Chen *et al.* 2016; Mottram and Taylor 1987). It should be noted that increasing filler loading level is not always preferred, as it can cause composite embrittlement, poor processability and high cost (Chen *et al.* 2016). Arambakam *et al.* (2013) found that fiber type, fiber volume fraction, fiber diameter, intrinsic thermal conductivity and fibers' through-plane orientations have significant impacts on the heat conduction of fibrous composite materials. Fu and Mai (2003) also studied the effects of fiber volume fraction, fiber length and orientation distributions on the thermal conductivity of short fiber composites. They found that the composite thermal conductivity increases almost linearly with the increase of fiber volume fraction. When the fiber thermal conductivity is high, the composite thermal conductivity increases significantly with the increase of mean fiber aspect ratio (or mean fiber length) and the decrease of mean fiber orientation angle and vice versa. The low thermal conductivity of silica fiber and MRR was beneficial for the thermal stability of the composites and their refractory application.

MORPHOLOGY ANALYSIS

Visual inspection

Visual inspection of the ablated composites was done using a digital camera, as shown in Fig. 16a-g. The photos revealed that the carbonaceous phase appears crumbly for 40 wt.% composite specimen while it was hardest and more difficult to scrape off by manual scratching for 55 wt.% and 65 wt.% composite specimens. After ablation, fine cracks and surface protruding only appeared in the 40 wt.% SSF/MRR composite which shows visually increasing char layer thickness (Fig. 16b) with comparison to the 55 wt.% (Fig. 16c) and 65 wt.% (Fig. 16d) SSF/MRR composite counterparts. Char layer depth on the composite specimens was about 2.21 mm with clear cracks and surface blisters. However, SSF/MRR composite specimens with 55 wt.% and 65 wt.% fiber loading have, after ablation, flat surface and no noticeable protruding surfaces but they exhibited, far from the center of impingement, small and shallow pits of 6.45 mm diameter and 1.65 mm depth as shown in Fig. 16d. This adds to the fact that 55 wt.% and 65 wt.% SSF/MRR composite specimens were scarcely peeled off during ablation. Furthermore, the remarkable white central layer on the ablated surfaces could be related to amorphous SiO_2 (XRD analysis paragraph) resulting from the presence of short amorphous silica fiber as reinforcement in SSF/MRR composites (Figs. 16c-d). In addition, observation of ablated SSF/MRR composite specimen cross sections indicates the existence of long fissures spanning the entire samples length, these fissures are the result of thermal and mechanical stresses deforming the specimens during ablation process (Figs. 16e-g). These results demonstrate that higher SSF loading increases materials ablation resistance by controlling thermal expansion, material deformation resistance and strengthening of the integral composite structure (Qiu *et al.* 2005).

SEM morphology analysis

The morphology structure of SSF/MRR ablator before ablation test was investigated using SEM as depicted in Fig. 17, where the matrix resin and reinforced fiber are readily identified. It is noted that the short silica fibers are randomly distributed in the matrix (Fig. 17a). From Fig. 17b, it can be observed that the wet-out of the fibers by matrix is poor, there is little resin on the SSF surface.

The SEM micrographs of SSF/MRR composite specimens' surface morphology after ablation are given in Fig. 18.

The surface morphology of ablated SSF/MRR composites is covered with a number of craters and a large number of pores and pits which result from the decomposition of MRR matrix (Fig. 18a). Due to high heat flux, the silica fibers may attain locally melting state at the high ablation temperature leading to a frothy discontinues layer of silica with little or no carbon (Fig. 18a). But a large number of about 20 μm globules are present as well (Fig. 18b). These globules are distributed on the whole surface, which may result from molten silica freezing in the air. These observations are in accordance with

XRD and FTIR analysis of ablated specimens (Figs. 9 and 10). Carbonaceous debris around silica fibers may be observed in certain zones (Fig. 18c). The porous structure of the ablated sample enhances transpiration and vaporization, which in turn reduces heat penetration vertically and leads to less sub-surface decomposition and char formation during the ablation of composite specimens (Shi *et al.* 2016a; 2016b; Hsieh and Seader 1973; Torre *et al.* 2000).
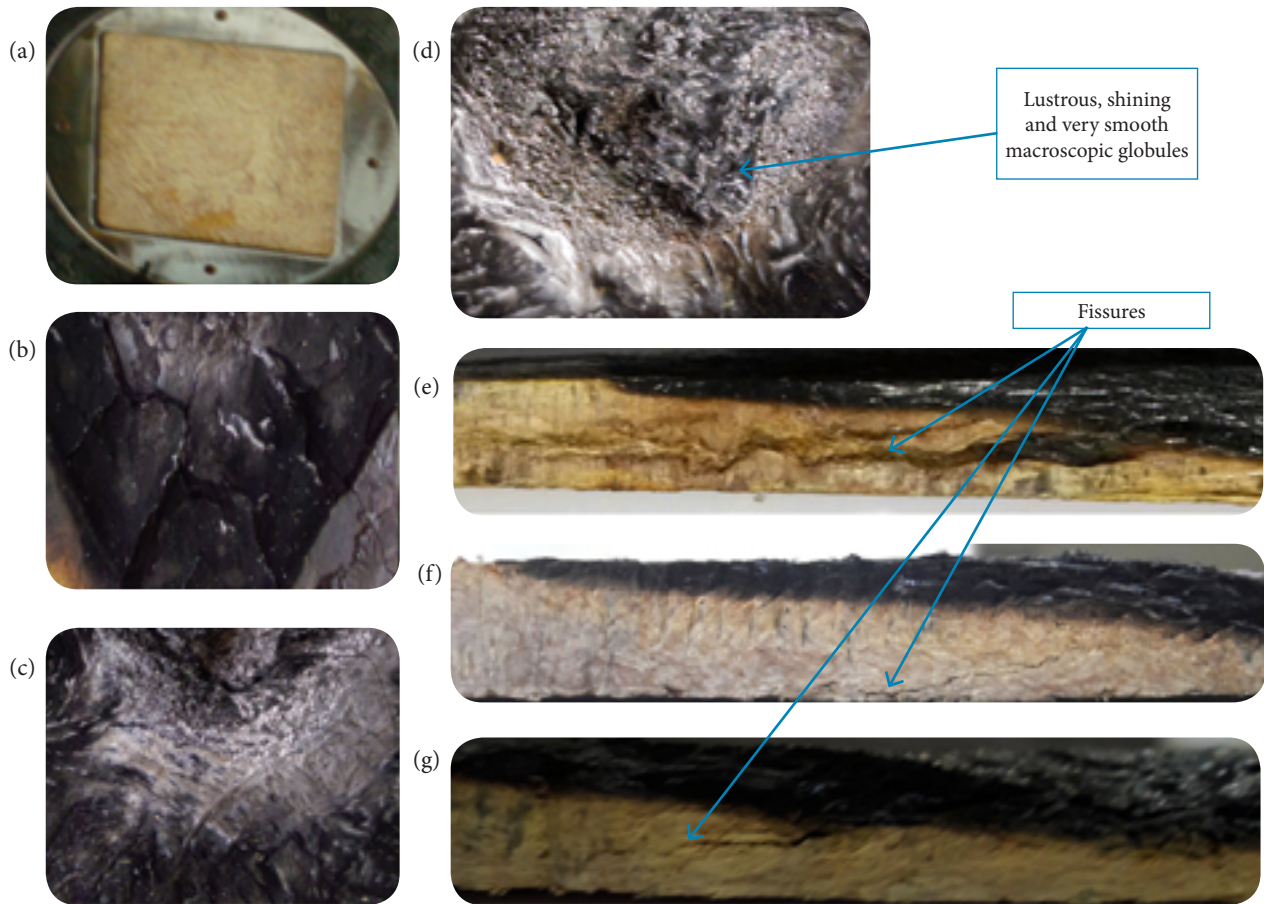

Figure 16. The surface morphology of SSF/MRR composite ablated specimens: (a) before ablation; ablated surfaces of (b) 40 wt.%, (c) 55 wt.%, and (d) 65 wt.% ablated specimens, respectively; and cross-sections of (e) 40 wt.%, (f) 55 wt.%, and (g) 65 wt.% ablated specimens composite, respectively.
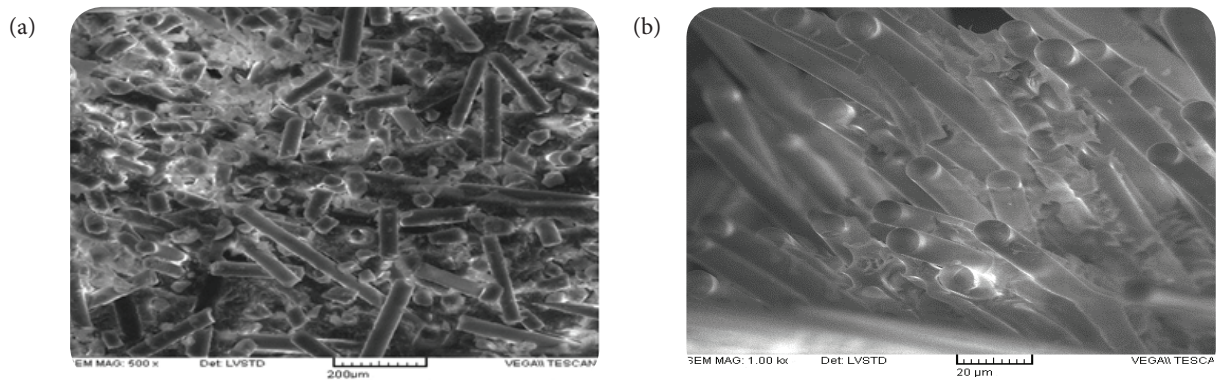

Figure 17. SEM micrographs of SSF/MRR ablator composite specimens before ablation: (a) random distribution SSF in composite; (b) poor wetting of fibers by matrix.
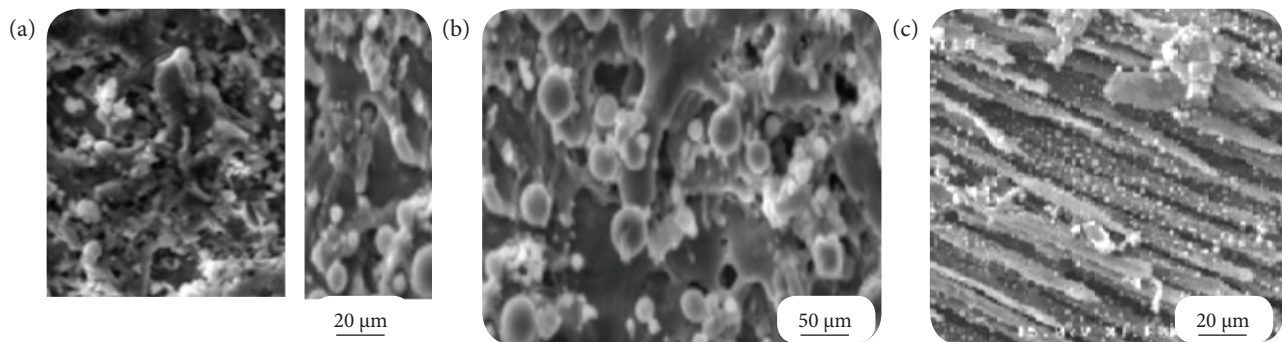
Figure 18. SEM micrographs of SSF/MRR composite specimens surface morphology after ablation: (a) very porous surface with craters and pits; (b) very porous surface with non-identified globules; and (c) surface with traces of bared fibers.

PYROLYSIS MECHANISM

Pyrolysis mechanism was not directly investigated in the present study. Nevertheless, the thermal and structural characterization of the ablated specimens together with the survey of previous studies allow to draw an overall analysis of the ablation behavior of SSF/MRR composite specimens, this behavior entails mainly the following steps (Torre *et al.* 2000; 1998a; 1998b; Mottram and Taylor 1987):

- Surface temperature rise and volatilization of water and unreacted species.
- Decomposition and significant weight loss of phenolic matrix.
- Char formation and eventually silica fibers melting and progression of ablation front.
- Damage of the resulting superficial char-fibers residue composite layer due to the combined effects of thermal stress, thermal shock, and the flame pressure, leading to the apparition of cracks, fissures and pits and recession of the ablated specimen surface at and around the oxyacetylene flame impingement point.
- The short duration of the oxyacetylene ablation test did not allow the formation of crystalline phase as a result of eventual chemical reaction or phase transformation.

The surface phenomena are described in Fig. 19, showing the pyrolysis events. The assumed chemical reactions between the pyrolysis gases and the reactive species taking place at the surface will be described with the following simple reaction pattern (Torre *et al.* 2000; 1998b; Mottram and Taylor 1987; Wong *et al.* 2015):

CONCLUSIONS

In the present study, SSF/MRR composites have been prepared with varying fiber concentrations. The effect of fiber concentration on composites ablative properties has been studied using a high-temperature flame test (oxyacetylene test). Composites thermal conductivity has been also investigated. The experimental study revealed the following conclusions:

- Chopped silica fibers have been almost evenly and effectively incorporated in the modified resole resin matrix using dispersion laboratory mixer and have been prepared through simple and low-cost hot-press molding without using coupling agents.
- The density of modified resole resin short silica fibers composites increased with increasing fiber content in accordance with the rule of mixture.
- The linear ablation rate of 40 wt.% silica fibers composite is higher than that of 65 wt.% and 55 wt.% composites. Its linear ablation rate is about 45% and 40% higher than the 65 wt.% and 55 wt.% silica fibers composites, respectively. Correspondingly, its mass ablation rate is about 57% and 32% higher than that of 65 wt.% and 55 wt.% silica fibers composites, respectively.
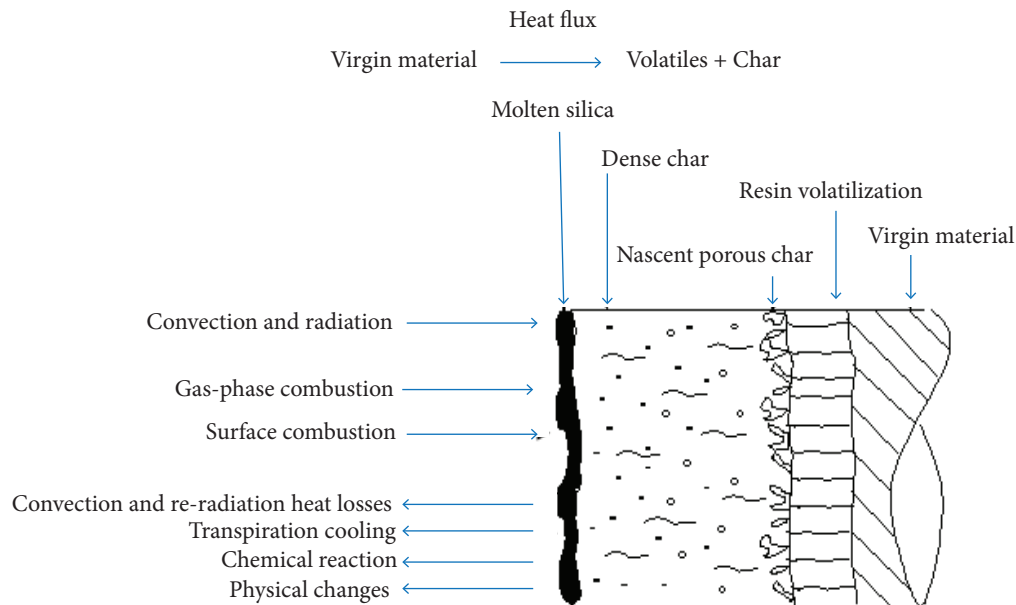
Figure 19. Schematic illustration of various zones during the ablation process.

- The ablative properties of 55 wt.% and 65 wt.% composites are almost close to each other. Thus, to obtain the best ablation resistance, fiber fraction must be carefully adjusted.
- Visual inspection of ablated surface indicates that higher fiber loading (i.e., 55 wt.% and 65 wt.%) can limit composite material fragmentation and also improve its anti-erosion performance. Moreover, the char produced from 40 wt.% silica fiber composites appears weak and brittle in comparison with that of 55 wt.% and 65 wt.% silica fiber composites. So, including silica reinforcement fibers in appropriate amounts into the ablative formula improves the mechanical resistance of the pyrolysis char, which plays an important role in insulating performance.
- The erosion resistance of the composite surface under an oxyacetylene flame was found to be significantly reduced with increasing fiber loading in SSF/MRR composites.
- The thermal conductivity of SSF/MRR composites is improved by adding SSF fibers to MRR matrix composites.
- X-Ray diffraction pattern and FTIR analysis of the ablated SSF/MRR composite indicate that no crystalline phases and α-cristobalite are generated under the test conditions and that no evidence of carbon-silica reaction takes place.
- The results of the oxyacetylene torch testing confirmed that SSF/MRR composites have the ability to fulfill the requirements of high-temperature applications.

AUTHOR'S CONTRIBUTION

Conceptualization, Elwan I, Jabra R and Arafeh MH; Methodology, Elwan I, Jabra R and Arafeh MH; Investigation, Elwan I and Arafeh MH; Writing – Original Draft, Elwan I and Jabra R; Writing – Review and Editing, Elwan I and Jabra R and Arafeh MH.

ACKNOWLEDGMENTS

REFERENCES

Arambakam R, Tafreshi HV, Pourdeyhimi B (2013) A simple simulation method for designing fibrous insulation materials. Materials and Design 44:99-106. doi: 10.1016/j.matdes.2012.07.058

Bahramanian AR, Kokabi M, Famili MHN, Beheshty MH (2006) Ablation and thermal degradation behavior of a composite based on resol type phenolic resin: process modeling and experimental. Polymer 47(10):3661-3673. doi: 10.1016/j.polymer.2006.03.049

Bigg DM (1986) Thermally conductive polymer compositions. Polymer composites 7(3):125-140. doi: 10.1002/pc.750070302

Ceballos-Mendivil LG, Cabanillas-López RE, Tánori-Córdova JC, Murrieta-Yescas R, Zavala-Rivera P, Castorena-González JH (2014) Synthesis and characterization of silicon carbide in the application of high temperature solar surface receptors. Energy Procedia 57:533-540. doi: 10.1016/j.egypro.2014.10.207

Chen H, Ginzburg VV, Yang J, Yang Y, Liu W, Huang Y, Du L, Chen B (2016) Thermal conductivity of polymer-based composites: fundamentals and applications. Progress in Polymer Science 59:41-85. doi: 10.1016/j.progpolymsci.2016.03.001

Chikhi M, Agoudjil B, Haddadi M, Boudenne A (2011) Numerical modelling of the effective thermal conductivity of heterogeneous materials. Journal of Thermoplastic Composite Materials 26(3):336-345. doi: 10.1177/0892705711424921

Da-Peng Z, Hong F (2008) Mechanical and high-temperature properties of glass fibers reinforced phenolic composites. Journal of Reinforced Plastic and Composites 27(13):1449-1460. doi: 10.1177/0731684407086613

Eslami Z, Yazdani F, Mirzapour MA (2015) Thermal and mechanical properties of phenolic-based composites reinforced by carbon fibers and multiwall carbon nanotubes. Composites Part A: Applied Science and Manufacturing 72:22-31. doi: 10.1016/j.compositesa.2015.01.015

Foley HC, Kane MS, Goellner JF (2002) New directions with carbogenic molecuar sieve materials. In: Pinnavaia TJ, Thorpe MF, editors. Access in nanoporous materials. Fundamental materials research. Boston: Springer. p. 39-58. doi: 10.1007/0-306-47066-7_4

Fu S-Y, Mai Y-W (2003) Thermal conductivity of misaligned short-fiber-reinforced polymer composites. Journal of Applied Polymer Science 88(6):1497-1505. doi: 10.1002/app.11864

Griffiths PR, Homes CC (2002) Instrumentation for far-infrared spectroscopy. In: Chalmers JM, Griffiths PR, editors. Handbook of vibrational spectroscopy. v 1. Chichester: John Wiley and Sons.

Hsieh C-L, Seader JD (1973) Surface ablation of silica-reinforced composites. AIAA Journal 11(8):1181-1187. doi: 10.2514/3.6890

Hu Y, Geng W, You H, Wang Y, Loy DA (2014) Modification of a phenolic resin with epoxy- and methacrylate-functionalized silica sols to improve the ablation resistance of their glass fiber-reinforced composites. Polymers 6(1):105-113. doi: 10.3390/polym6010105

Ismail IN, Ishak ZAM, Jaafar MF, Omar S, Zainal Abidin MF, Ahmad Marzuki HF (2009) Thermomechanical properties of toughened phenolic resol resin. Solid state science and technology 17(1):155-165.

Kang TJ, Hwang SD (1996) Effect of matrix toughening on the mechanical properties of glass fibre reinforced composite. Polymers and polymer composites 4(4):217-224.

Kim M, Choe J, Lee DG (2016) Development of the fire retardant glass fabric/carbonized phenolic composite. Composite Structures 148(15):191-197. doi: 10.1016/j.compstruct.2016.04.003

Lochte HW, Strauss EL, Conley RT. (1965) The thermo-oxidative degradation of phenol–formaldehyde polycondensates: thermogravimetric and elemental composition studies of char formation. Journal of Applied Polymer Science 9(8):2799-2810. doi: 10.1002/app.1965.070090814

Mottram JT, Taylor R (1987) Thermal conductivity of fibre-phenolic resin composites. Part I: thermal diffusivity measurements. Composites Science and Technology 29(3):189-210. doi: 10.1016/0266-3538(87)90070-4

Mouritz AP, Gibson AG (2006) Fire properties of polymer composite materials. 1st ed. Amsterdam: Springer.

Nair CPR (2004) Advances in addition-cure phenolic resins. Progress in Polymer Science 29(5):401-498. doi: 10.1016/j.progpolymsci.2004.01.004

Najim TS, Naji AM, Barbooti MM (2008) Thermal and ablative properties of Ipns and composites of high ortho resole resin and difurfurylidene acetone. Leonardo Electronic Journal of Practices and Technologies 7(13):34-46.

Ommati M, Ahmadi IF, Davachi SM, Motahari S (2011) Erosion rate of random short carbon fibre/phenolic resin composites: modelling and experimental approach. Iranian Polymer Journal 20(12):943-954.

Pilato L, editor (2010) Phenolic resins: a century of progress. Berlim: Springer-Verlag. doi: 10.1007/978-3-642-04714-5

Qinghua C (1992) Ablative Thermal Protection Structure Design of Ballistic Reentry spacecraft. (ID (RS) T-0623-92). FASTC Technical Report.

Qiu J, Cao X, Tian C, Zhang J (2005) Ablation performance of a novel super-hybrid composite. J Mater Sci Technol 21(2):269-273.

Scian AN, Volzone C (2001) Novel SiO2-C composite adsorptive material. Bol Soc Esp Cerámic Vidrio 40(4):279-285.

Shafizadeh JE, Guionnet S, Tillman MS, Seferis JC (1999) Synthesis and characterization of phenolic resole resins for composite applications. Journal of Applied Polymer Science 73(4):505-514. doi: 10.1002/ (SICI)1097-4628(19990725)73:4<505::AID-APP6>3.0.CO;2-L

Shen M-X, Cui Y-X, He J, Zhang Y-M (2011) Thermal conductivity model of filled polymer composites. International Journal of Minerals, Metallurgy and Materials 18(5):623-631. doi: 10.1007/s12613-011-0487-9

Shi S, Liang J, He R (2015) Thermal decomposition behavior of silica-phenolic composite exposed to one-sided radiant heating. Polymer composites 36(8):1557-1564. doi: 10.1002/pc.23074

Shi S, Gong C, Liang J, Fang G, Wen L, Gu L (2016a) Ablation mechanism and properties of silica fiber-reinforced composite upon oxyacetylene torch exposure. Journal of Composite Materials 50(27):3853-3862. doi: 10.1177/0021998315626504

Shi S, Li L, Liang J, Tang S (2016b) Surface and volumetric ablation behaviors of SiFRP composites at high heating rates for thermal protection applications. International Journal of Heat and Mass Transfer 102:1190-1198. doi: 10.1016/j.ijheatmasstransfer.2016.06.085

Shulock H, Saffadi RR (1982) High Silica and Quartz. In: Lubin G, editor. Handbook of Composites. 1st ed. New York: Springer. p. 160-170.

Torre L, Kenny JM, Boghetich G, Maffezzoli A (2000) Degradation behavior of a composite material for thermal protection systems Part III Char characterization. Journal of Materials Science 35(18):4563-4566. doi: 10.1023/A: 1004828923152

Torre L, Kenny JM, Maffezzoli AM (1998a) Degradation behavior of a composite material for thermal protection systems Part I Experimental characterization. Journal of Materials Science 33(12):3137-3143. doi: 10.1023/A:1004399923891

Torre L, Kenny JM, Maffezzoli AM (1998b) Degradation behavior of a composite material for thermal protection systems Part II Process simulation. Journal of Materials Science 33(12):3145-3149. doi: 10.1023/A:1004352007961

Trick KA, Saliba TE (1995) Mechanisms of the pyrolysis of phenolic resin in a carbon/phenolic composite. Carbon 33(11):1509-1515. doi: 10.1016/0008-6223(95)00092-R

Wang CH, Wei QH, Wang HS, Li L, Luan Q, Liao R (2012) Dielectric properties of silica fiber reinforced silica composites. Key Engineering Materials 512-515:547-550. doi: 10.4028/www.scientific.net/KEM.512-515.547

Wilkie CA, Morgan AB (2009) Fire retardancy of polymeric materials. 2nd ed. Boca Raton: Taylor and Francis Group, CRC Press.

Wong H-W, Peck J, Bonomi RE, Assif J, Panerai F, Reinisch G, Lachaud J, Mansour NN (2015) Quantitative determination of species production from phenol-formaldehyde resin pyrolysis. Polymer Degradation and Stability 112:122-131. doi: 10.1016/j.polymdegradstab.2014.12.020